Macromolecules
ARTICLE

Macromolecules **2010**, *43*, 5323–5329 **5323**
DOI: 10.1021/ma100056j

Crystallization and Phase Separation of Branched Low Molecular Weight Polyethylene/Ultrahigh Molecular Weight Polyethylene Blend under a Controlled Temperature Gradient

Duigong Xu,[†] Yuezhen Bin,*[,†,‡] and Ping Tang[†]

[†]*Department of Polymer Science and Engineering and* [‡]*State Key Laboratory of Fine Chemicals, School of Chemical Engineering, Dalian University of Technology, Zhongshan Road 158, Dalian 116012, China*

Received January 9, 2010; Revised Manuscript Received May 8, 2010

ABSTRACT: Crystallization and phase separation of polyethylene blend were first studied under a controlled temperature gradient (T-gradient) condition. Branched low molecular weight polyethylene (B-LMWPE) and ultrahigh molecular weight polyethylene (UHMWPE) blend films were prepared by casting the blend solutions on the T-gradient stage and then evaporating the solvent. The morphological evolution of blend films was investigated in detail. The blend films showed a continuous gradients surface. With increasing temperature, the degrees of crystallinity for both of the B-LMWPE and UHMWPE decreased in the blend films. The results indicated that phase separation behavior of B-LMWPE and UHMWPE blend with composition 10/1 or 5/1 occurred in both of solution and gel, and the phase separation was prior to crystallization. It is suggested that phase separation should induce molecular ordering and crystallization in the B-LMWPE/UHMWPE blend in the initial stage, and the phase separation and crystallization compete with each other in the later period. Another fact is that high viscosity of blend solution plays a more important role in phase separation rather than in crystallization, and it will be the main disincentive in inhibiting the Marangoni phenomenon when the composition of UHMWPE increases in the blend.

Introduction

Gelation/crystallization is an excellent method to prepare high-modulus and high-strength polyethylene. This method developed by Smith and Lemstra[1−3] has caused significant impacts on the polymer science. They demonstrated that ultradrawing ability of ultrahigh molecular weight polyethylene (UHMWPE) was attributed to a reduced number of entanglements per molecule in solution-cast/spun polymers in comparison with those obtained from melts. Besides using UHMWPE, Matsuo et al.[4−7] applied this method to prepare the blend films of UHMWPE and branched low molecular weight polyethylene (B-LMWPE), since the viscosity of solution became a drastic decrease with increasing content of B-LMWPE. They investigated the crystallization behavior of two components in the blend film. In this kind of polymer blend system, crystallization and phase separation are two principal issues. They govern the structure and morphology and ultimately affect the properties of materials. It has been demonstrated that when one component of the blend is crystallized, there is an interaction between crystallization and phase separation, and it is necessary to consider correlative relationship of the two phenomena.

According to recent reports,[8−10] phase separation and crystallization can interfere and compete with each other in crystalline polymer blend at the early stage. Matsuo et al.[11] have pointed out that no crystallization occurred in the initial stage of liquid−liquid phase separation for B-LMWPE or UHMWPE solutions at a desired temperature lower than its gelation temperature. It is believed that phase separation played as a driving force to cause gelation/crystallization. On the other hand, Graham et al.[12] demonstrated that crystallization was a viable mechanism for locking in the two-phase structure of a crystalline polymer solution in thermally induced phase separation. Of course in the B-LMWPE/UHMWPE blend system, the situation will become more complicated because physical gelation of polymer solution could affect crystallization and phase separation. Bansil et al.[13] used a system of gelatin, water, and methanol to observe the effect of gelation on phase separation. When the quenching temperature was below the gelation temperature for pure gelatin, the gelation was found to halt the phase separation process. For quenching to higher temperatures, the phase separation was found to be similar to classical, nongelling mixtures. In addition, the effect of viscosity of the solutions on phase separation also needs to be considered because the coarsening droplets could be frozen by the solidification of the matrix phase via viscoelastic effects of polymer chains.[14,15] Namely, the slow fluid component (the UHMWPE-rich phase) could not catch up with the deformation rate of phase separation itself and behaved like a high-viscosity body[15] when the concentrations were large enough.

There is no doubt that those above excellent works have revealed the correlative relationship between crystallization and phase separation in the crystalline polymer blend. However, for the complex system such as UHMWPE and B-LWMPE blend, it is still not easy to understand the morphological evolution of polymer blend under different temperature conditions. The present work extends to combinatorial methods for studying the morphological evolution of B-LMWPE/UHMWPE blend involved crystallization and phase separation during the annealing period. Combinatorial methods[16−21] provided us with a new idea that is to prepare the sample with gradient structure under a temperature gradient (T-gradient). Based on the previous work,[4,11,22−24] the T-gradient was kept at an appropriate range ensuring the coexistence of polymer solution and gels on the same

*Corresponding author: Fax +86 411 39893638; e-mail binyz@dlut.edu.cn.

Published on Web 05/19/2010

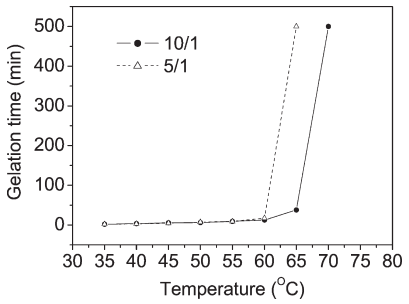

Figure 1. Gelation time of the 10/1 and 5/1 B-LMWPE/UHMWPE well-blended solutions at different temperatures.

stage. The temperature range containing the gelation temperature of the blend was lower than the melting point of B-LMWPE. This means that the blend would form gels on the stage where the temperature was lower than the gelation temperature, and it would be kept as solution at the high temperature side on the stage for the period neglecting the evaporation of solvent. In this study, the final dry film, which was partly annealed from gels and partly from the solution by evaporating solvent, was investigated by polarizing microscope, scanning electron microscopy (SEM), differential scanning calorimetry (DSC), and Fourier transform infrared (FTIR) observations.

Experimental Methodology

Materials. The samples were prepared by using UHMWPE (Hizex Million 630M) with a viscosity-average molecular weight of 6.3×10^6 and B-LMWPE (Sumikathene G201) with a viscosity-average molecular weight of 4×10^4 and containing 2.5 degrees of short chain branching. The compositions of B-LMWPE/UHMWPE chosen were 10/1 and 5/1 in weight ratio. Solvent was xylene (mixture of isomer, commercial).

Preparation of T-Gradient Library. A xylene solution containing UHMWPE and B-LMWPE was prepared by heating the well-blended polymer/solvent mixture at 130 °C for 1 h under nitrogen. The concentration of UHMWPE against solvent was fixed to be 10 mg/mL, and the amount of B-LMWPE was determined as relative ratio to UHMWPE, while the compositions of B-LMWPE and UHMWPE blend were 10/1 and 5/1.

Then 15 mL of hot homogenized B-LMWPE/UHMWPE blend solution was poured onto the T-gradient stage to form a film with ca. 150 μm thickness. Then xylene was allowed to evaporate from the blend under T-gradient conditions. It took about several hours to form a dry film. Crystallization and phase separation of B-LMWPE/UHMWPE blend occurred during this process. The drying time was dependent on the concentration of solutions. Then the film was divided into several pieces depending on the position of the T-gradient stage, corresponding to the annealing temperature, and each piece of specimen was investigated separately. Besides, noncombinatorial experiments of 10/1 composition at the selected temperature points were done for confirming the validity of the method.

In order to determine the T-gradient range, the gelation temperature and the gelation time of hot B-LMWPE/UHMWPE blend solutions were measured first. 5 mL of well-blended solution was poured into a glass tube which was immerged in silicon oil at a desired temperature. The time until the solution did not flow under its own weight by tilting the tube was defined as the "gelation time". The highest temperature at which the onset of gelation occurred within 1 h was defined as the "gelation temperature". This method was a little different with the other reports.[11,25,26] Figure 1 depicts the gelation time at the different temperatures. It indicates that the gelation temperatures of B-LMWPE/UHMWPE blend with 10/1 compositions is about 65 °C and 5/1 is about 60 °C. It is considered as the reference to design the T-gradient range.

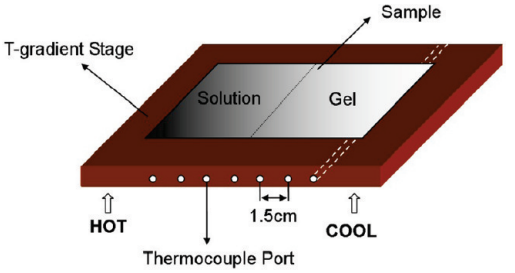

Figure 2. Schematic drawing of the T-gradient stage employed for the formation of a T-gradient library.

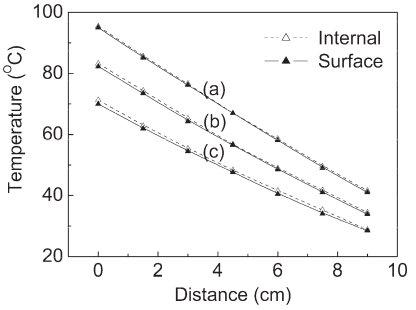

Figure 3. Internal and surface temperatures at different positions of the stage. The heater was set at (a) 100, (b) 90, and (c) 80 °C while the cooler was at 25 °C constantly.

Design and Calibration of the T-Gradient Stage. Referring to the reports from other researchers,[27−30] we chose an aluminum plate as the stuff to design a T-gradient field (see Figure 2). This T-gradient stage employed a heater and a cooler, which resulted in a linear T-gradient range from one side to another. The heater and cooler were controlled independently by two thermostats to make the temperature range of the stage controllable. The distance between two thermocouple ports was 1.5 cm. The first port in the left was set at 0 cm, while the seventh port was 9 cm, which is much larger than those stages reported before.[16,17,27]

Although the internal temperature of the stage could be obtained easily, the surface temperature, which is valid and close to the sample temperature, was difficult to measure directly. So the "simulation method" was adopted to estimate the surface temperature. The so-called simulation method was that, first, a polyethylene film (simulating the blend film) was firmly attached on the surface of the stage, and then the probe was inserted into the gap between film and stage at the positions just above each thermocouple port. The surface temperatures at different positions of the stage were determined. Then the differences between the internal temperature and the surface one at the different positions were calibrated one by one. Figure 3 shows the results of calibration when the heater was kept at different temperatures, such as 80, 90, and 100 °C, while the cooler was constant, at 25 °C. With increasing heating temperature, the T-gradient range increases, and the surface temperature is more close to the internal temperature. Especially for the heater kept at 100 °C, the internal temperature is only a little higher than the surface temperature with difference less than 1 °C. The difference is attributed to convection airflow and radiant heat loss. It means that there is a T-gradient along the vertical plane of the stage. However, this vertical temperature difference is quite slight, as can be neglected for our research system.

According to the obtained gelation temperature and the melting point of B-LMWPE in the preliminarily experiment, the T-gradient range of this study was set from 40 to 95 °C, where heater was kept at 100 °C and cooler at 25 °C. In this T-gradient, surface and internal temperatures at every port

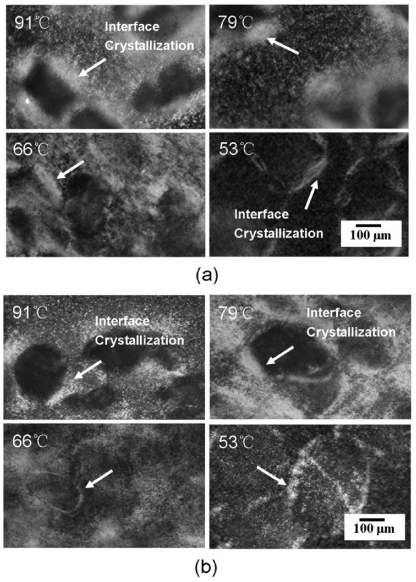

Figure 4. Polarizing microscope images of the dry blend films with 10/1 of B-LMWPE/UHMWPE at different temperatures, corresponding to 91, 79, 66, and 53 °C, respectively. Scale bar in all images is 100 μm. (a) from combinatorial experiments and (b) from noncombinatorial experiments.

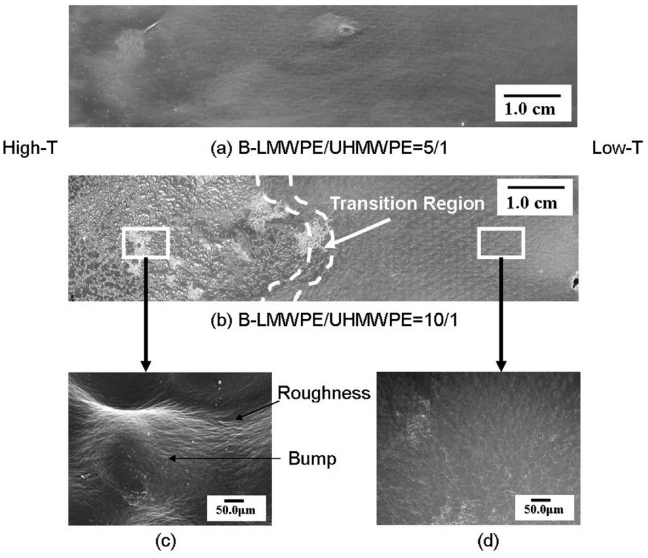

Figure 5. Morphology of dry blend films with different compositions. (a) and (b) are photographs from a digital camera. (c) and (d) are the SEM images of surfaces of the B-LMWPE/UHMWPE = 10/1 blend dry film at different positions corresponding to 85 and 53 °C, respectively. Scale bar is 50 μm in (c) and (d).

could be considered as the same profile as shown in Figure 3a. In addition, the temperature was linear change in the whole range. The T-gradient, X_g can be easily calculated from eq 1, where T_d is the temperature difference and D is the distance between the two ends. The surface temperature of any point on the stage can be obtained.

$$X_g = \frac{T_d}{D} \quad (1)$$

From the gelation time at different temperatures as shown in Figure 1, it can be seen that the gelation temperature is 65 °C for 10/1 composition and 60 °C for 5/1. The time is more than 500 min when the original solution of 10/1 composition gels at about 70 °C, which is far beyond the solvent evaporation time. Therefore, the blend is always in solution state above 65 °C and in gel state below the temperature if the solvent is not evaporated as shown in Figure 2. Of course, the blend was dried by evaporating the solvent.

Characterization of Films with Gradient Structure. The morphologies of the film produced under T-gradient conditions were obtained by a Nikon polarizing microscope (X2TP-11). Further structure analysis was carried out by SEM. The cross sections of films were freeze-fractured under liquid nitrogen. These samples were gold sputtered and analyzed using SEM (JEOL JSM-7600).

Phase separation and crystallization behaviors were also investigated in terms of melting endotherms of DSC curves. DSC measurements were performed at a heating rate of 5 °C/min from 20 to 160 °C in a N_2 atmosphere by using DSC-204 (NETZSCH). The weight of samples sealed in aluminum pans was 9−10 mg.

FTIR spectroscopy (AVATAR330-FTIR, Nicolet) was carried out to verify the change of relative crystallinity in the range of bands from 1200 to 1400 cm^{-1}.

Results and Discussion

Noncombinatorial Experiments for Validation. Before discussing the combinatorial experiments results, noncombinatorial experiments of 10/1 composition at selected temperature points were done for validation. A part of blend solutions was casted on the T-gradient stage to form a T-gradient structure film. The residual solutions of the same solutions were casted into several aluminum dishes which were set on the several constant temperature stages to evaporate the solvent. The temperature points of samples correspond to 91, 79, 66, and 53 °C. Then the morphology was observed. Figure 4 shows the polarizing microscope images of the two kinds of films obtained on the T-gradient stage and corresponding constant temperature stages. Figure 4a,b shows quite similar morphology characteristics at the same temperature points. For instance, a clear crystallization occurred at the interface, called interface crystallization. Another important feature of the two kinds of samples is that the interface crystallization seems to be stronger on high-temperature point. We also compared the results of DSC measurement and FTIR spectra for above samples. Almost the same results were obtained, and we did not show them here. Those results mean that the T-gradient brought extremely small interfere on the morphology evolution of the blend compared to the preparation method under the constant temperature for the B-LMWPE/UHMWPE blend system. Namely, the combinatorial method is feasible in this study. Therefore, the combinatorial experiments results were mainly discussed below.

Surface Characteristics of B-LMWPE/UHMWPE Blend Films under a T-Gradient. Figure 5 shows the morphology of dry blend films with the 10/1 and 5/1 compositions. These resultant films appear an obvious gradient surface, especially in the dry film with B-LMWPE/UHMWPE = 10/1 composition (see Figure 5b). The transition region obviously exists between the solution and gel regions of the blend at about 65 °C. The surface roughness at the high temperature is associated with the Marangoni effect.[31,32] On the basis of this concept, the formation of the roughness can be explained. When the solvent was evaporated rapidly, there was a concentration fluctuation. The presence of concentration fluctuation in blend would naturally cause the interfacial tension gradient which drove liquid flowing from the regions of low interfacial tension to the high one. This behavior made the surface of the solution contract and, ultimately, the formation of rough surface. Besides, the surface roughness

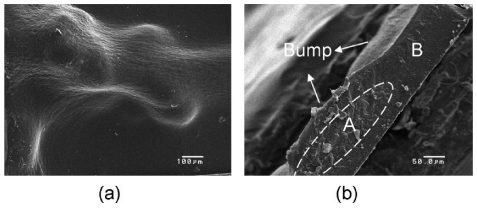

Figure 6. SEM images of surface (a) and cross section (b) of bump area obtained from 10/1 composition dry film at high temperature. Domain A corresponds to UHMWPE-rich phase; domain B corresponds to B-LMWPE-rich phase.

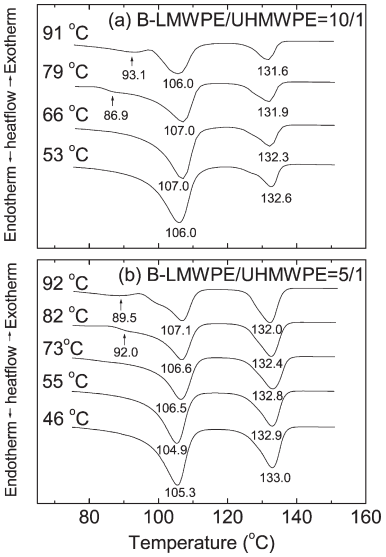

Figure 7. DSC curves for the samples at different positions on the T-gradient stage, where the compositions were 10/1 (a) or 5/1 (b).

is more obvious at high-temperature end because the network elasticity arising from the gelation can suppress concentration fluctuation. This result indicates that gelation is an important factor in inducing the surface morphology. Further, there are lots of surface bumps at the high-temperature end; in contrast, no bumps are observed at the low-temperature end as shown in the SEM images (Figure 5c,d). The form mechanism of the bumps will be discussed later.

Figure 6 shows SEM images for the surface and cross section of the film with large bumps. It can be seen that the bumps are mainly formed by UHMWPE domains where the fibrils of UHMWPE can be observed clearly in the cross section. The flat part shows smooth cross section, suggesting that it mainly contains B-LMWPE component as domain B in Figure 6b.

Crystallization and Phase Separation Behaviors. Figure 7 shows DSC curves for the specimens sampled at various annealing temperatures on the T-gradient stage, where the ratios of LMWPE/UHMWPE were 10/1 and 5/1. These samples captured from the B-LMWPE/UHMWPE = 10/1 film correspond to the annealing temperatures: 91, 79, 66, and 53 °C on the T-gradient stage and from B-LMWPE/UHMWPE = 5/1 film correspond to 92, 82, 73, 55, and 46 °C. The thermal characteristic is obviously dependent upon the annealing temperature. The DSC curve of the annealed sample shows two main endothermic peaks. Judging from the melting points of pure UHMWPE dry gel film (139 °C) and B-LMWPE(100 °C),[4] the peaks at higher (131.6−133 °C) and lower (104.9−107.1 °C) temperature sides for both 10/1 and 5/1 are associated with the melting points of

Table 1. Heat of Fusion and Crystallinity of B-LMWPE/UHMWPE Films with Different Ratios under the T-Gradient

	B-LMWPE		UHMWPE	
T (°C)	Δh_{f1} (J/g)	X_1 (%)	Δh_{f2} (J/g)	X_2 (%)
	B-LMWPE/UHMWPE = 10/1			
53	114.1	39.8	228.1	79.5
66	102.8	35.8	225.5	78.6
79	92.5	32.2	212.1	74.0
91	73.0	25.5	179.9	62.7
	B-LMWPE/UHMWPE = 5/1			
46	92.5	32.2	224.6	78.3
55	89.3	31.1	208.5	72.7
73	84.2	29.4	216.2	75.4
82	72.6	25.3	210.7	73.5
92	62.9	21.9	187.8	65.5

UHMWPE and B-LMWPE. The melting point of UHMWPE crystallites within the both blends is much lower than the melting point of UHMWPE homopolymer gel film, and the point of B-LMWPE is higher than pure B-LMWPE sample. It indicates that most of UHMWPE and B-LMWPE chains crystallized independently under heat treatment, but a few chains of the two components entangled and formed cocrystallization. This behavior is consistent with the result for the samples prepared by quenching to room temperature as reported before.[4] More importantly, there are only two sharp peaks in the DSC curve. This thermal characteristic indicates that phase separation of the blend was obvious, and it was prior to crystallization.

Incidentally, further observation shows that a shoulder peak appears in the low-temperature side in DSC curves marked by the arrow. As found in previously reported research,[33] B-LMWPE would appear the secondary crystallization after nonisothermal crystallization and the long branched chains could participate in crystallization above about 80 °C. Here, it is attributed to the role of Marangoni effects, which brought instability resulting in nonisothermal crystallization at the high temperature. It also explains that why the shoulder peak was not found in the sample at the low-temperature side of the T-gradient stage.

The detailed results estimated by the DSC curves in Figure 7 are summarized in Table 1, in which heat of fusion and crystallinity are listed for the different temperature points. Each heat of fusion was calculated by the relationship: heat of fusion (Δh_f) observed value/content of UHMWPE (or B-LMWPE) based on individual peak concerning UHMWPE and B-LMWPE crystallites. The crystallinity (X_c) was calculated from eq 2 by assuming the heat fusion of 100% crystalline polyethylene ($\Delta h_{f\text{-}PE}$) to be 286.8 J/g.[34]

$$X_c = \frac{\Delta h_f}{\Delta h_{f\text{-}PE}} \times 100\% \quad (2)$$

As shown in Table 1, the crystallinity of both compositions decreased as the temperature rising because crystal nucleus was difficult to be formed or unstable ascribed to the violent molecular thermodynamic movement at the higher temperature regions. Of course, UHMWPE with linear chains and high molecular weight can achieve a higher degree of crystallinity than B-LMWPE.

To obtain further confirmation, FTIR spectroscopy were also detected for studying the crystallization behavior of B-LMWPE/UHMWPE = 10/1 blend film. Figure 8 shows that the FTIR spectra for the film annealed at different

temperatures on the T-gradient stage. The relative crystallinity was analyzed based on the FTIR spectra. The absorption peak at 2019 cm^{-1} corresponding to methylene peak was used as the internal standard because it was inert to the change of crystallinity, and the absorption peak at 1894 cm^{-1} was chosen as analysis peak which corresponded to crystalline

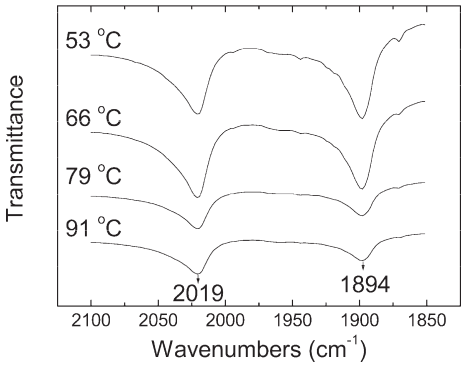

Figure 8. FTIR spectra for B-LMWPE/UHMWPE = 10/1 dry blend film annealed at different temperatures.

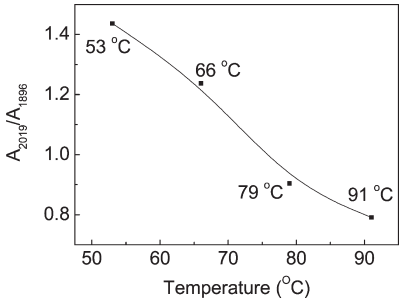

Figure 9. Relative crystallinity of the 10/1 composition blend film at different temperatures.

combination mode.[35,36] The relative crystallinity of PE was calculated from eq 3, where X_c is the relative crystallinity, A_i is the area of the absorption peak at 1894 cm^{-1}, A_s is the area of peak at 2019 cm^{-1}, and k is the proportional factor measured by using the known crystallinity of samples. In this work, the relative crystallinity can be represented by A_i/A_s. The most important advantage for this method is that the influence of thickness could be eliminated. Figure 9 presents that the relative crystallinity of samples calculated with eq 3. It indicates that the relative crystallinity of polyethylene decreases from low temperature to high temperature. This result is consistent with DSC measurement.

$$X_c = \frac{A_i}{A_s} k \tag{3}$$

In order to investigate the relationship between phase separation and crystallization under the T-gradient in details, cross sections of dry blend films were observed by SEM. Figure 10 shows two examples, obtained from the film of 10/1 composition at 91 and 53 °C. Phase separation for both samples occurred obviously. The UHMWPE fibrils formed networks in the UHMWPE-rich phase. This loose structure is a trail of solvent evaporation. However, two samples provided different morphology. In particular, the phase interface became unclear at the higher temperature compared to the lower one.

Cross sections of the B-LMWPE/UHMWPE blend films of 5/1 composition were also observed by SEM. As seen in Figure 11, compared with the sample of 10/1, the cross section became much smooth in 5/1 composition. In addition, there was no obvious transition region and roughness in the film with 5/1 composition (refer Figure 5a). It indicates that the entanglements of UHMWPE molecular chains restricted Marangoni instability in the whole annealing process in both solution and gels, and even the droplet growth was hampered as increasing UHMWPE content.

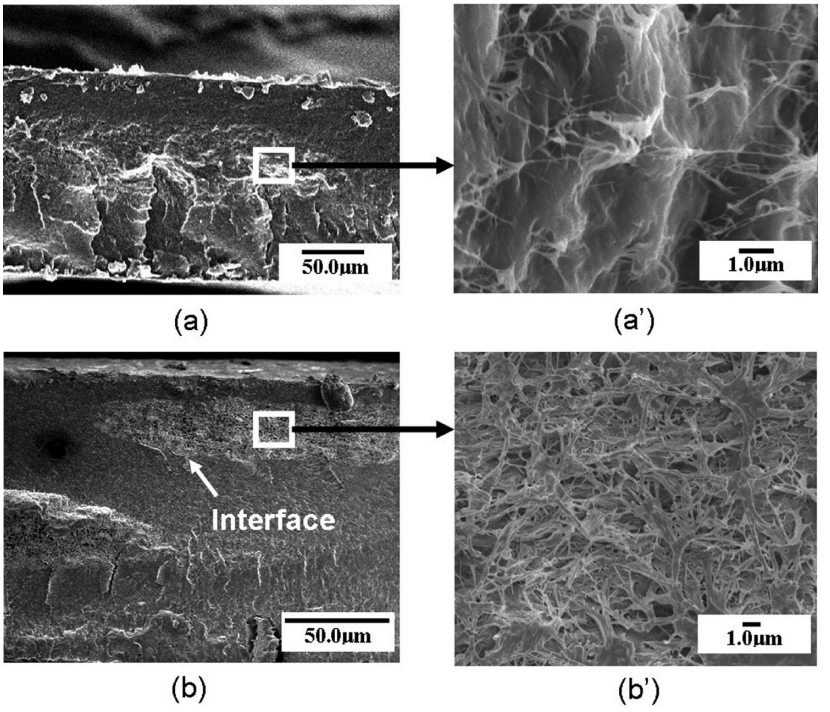

Figure 10. SEM images of cross sections of 10/1 dry blend film with the temperature at 80 °C (a, a′) and 53 °C (b, b′). Scale bar in (a, b) = 50 μm; (a′, b′) = 1 μm.

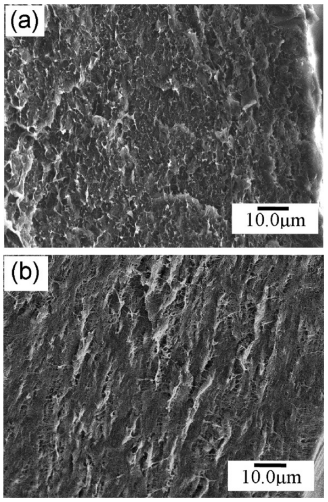

Figure 11. SEM images of cross sections of 5/1 dry film annealed at temperature (a) 92 °C and (b) 46 °C.

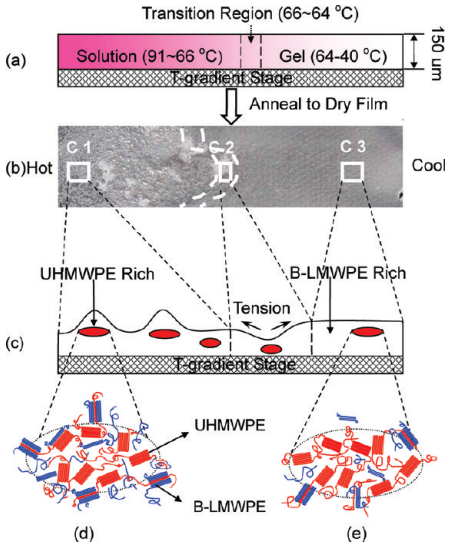

Figure 12. Schematic representation of the typical T-gradient structure for 10/1 blend film. (a) Cross-section sketch of the blend casted onto the T-gradient stage. (b) Photograph of the dry blend film formed on the T-gradient stage. (c) Cross-section scheme of the dry blend film corresponding to the different configurations in (b).

But microphase separation occurred. On the other hand, for 10/1 and 5/1 blends, the difference of crystallinity of UHMWPE or B-LMWPE calculated from DSC profile was no obvious. These results demonstrate that the high viscosity of UHMWPE solution plays an important role in phase separation rather than in crystallization. Figure 5 also shows that there are few bumps in the B-LMWPE/UHMWPE blend film of 5/1 composition. It suggests that the effects of gelation and viscosity on the morphological evolution of blend films were interrelated. In sum, when the viscosity of the blend is low, gelation plays a leading role in inhibiting the Marangoni phenomenon, but when the viscosity increases, the main disincentive is from the viscosity effect.

Speculation of Mechanism of the Morphological Evolution. On the basis of the results from Figures 4−11, we proposed a mechanism to illustrate the formation of the typical gradient structure for the B-LMWPE and UHMWPE blend as scheme as shown in Figure 12.

As shown in Figure 12b, the gradient film of 10/1 composition can be divided into three kinds of configurations. Configuration 1 (C1) with large roughness and many bumps might be produced through complex evolution from solution. At the early stage of the high-temperature end, phase separation occurred due to the increasing local concentration of blend solution when the solvent was evaporated rapidly. The velocity field was induced by the gradient interface tension. Then small droplets of UHMWPE phase were absorbed through diffusion into the larger ones due to self-similar growth. At high temperature, the Marangoni effect was significant, making the growth violent, and bumps occurred soon after due to the surface contraction. However, a high viscosity of UHMWPE solution managed the later process as solvent evaporating. It led to that a few of B-LMWPE could not escape from the UHMWPE-rich phase but participated in crystallization of UHMWPE; more B-LMWPE formed the interface with UHMWPE and co-crystallized at the same time, as shown Figure 12d. When the viscosity of solution was high enough, the bumps were "frozen" in the nonequilibrium morphology and eventually served as the final product. These bumps could not be healed by their own gravity.

Configuration 2 (C2), which looks like a gully, is a transition region. This configuration may be formed due to the reverse tensions. One was from the surface contraction at higher temperature end, and the other was from the surface tension of gels. The surface of the blend film could be easily torn by the two tensions.

Configuration 3 (C3) with few roughness and bumps was suggested to be the result of strong intermolecular forces and network structures in gels, which eliminated Marangoni effects. Since no crystallization occurred in the initial stage of liquid−liquid phase separation of the UHMWPE and B-LMWPE solutions,[11] the droplets were possibly induced by a deep temperature jump.[15] The droplets grew up quickly until the solution formed gels, and then they were frozen. The evolution was very gentle at low evaporation rate of solvent. Most of B-LMWPE molecules had enough time to separate from the UHMWPE-rich phase. Only a few of them cocrystallized with UHMWPE molecules in the UHMWPE phase. Of course, interface crystallization still existed owing to that some long chains of UHMWPE could easily extend into the B-LMWPE phase to being as nucleus (see Figure 12e).

As discussed above, although this complex situation such as the introduction of the temperature gradient and gelation cannot be entirely explained by this mechanism, it is still a useful clue to elucidate the morphology evolution of the polymer blend.

Conclusions

The crystallization and phase separation behaviors of the B-LMWPE/UHMWPE blend films prepared by using gelation/crystallization methods from solution were investigated under a controlled temperature gradient condition in this research. The results showed that a gradually varying aggregation structures formed in a film under the temperature gradient. There were many bumps and much obvious surface roughness at the high-temperature side, while the surface was much smooth and the structure was much compact at the low-temperature side. As increasing temperature, the degree of crystallinity decreased in both of B-LMWPE and UHMWPE. The results of DSC measurements demonstrated that phase separation of the blend occurred in both solutions and gels, and it was prior to crystallization, but a few of UHMWPE and B-LMWPE would cocrystallize later. From above results, it is suggested that phase

separation induce crystallization in the B-LMWPE/UHMWPE blend in the initial stage, and then they compete with each other in the later period. Another fact for 10/1 blend is that Marangoni instability relating of high viscosity of UHMWPE solution is necessary to be considered simultaneously to explain the complex evolution at late stage of phase separation in solution, while the droplet growth is restricted by gelation at the low-temperature end. It also indicates that the viscosity effect of solution is more significant on the phase separation rather than on crystallization, and it will play a leading role in inhibiting the Marangoni phenomenon when the composition of UHMWPE increases in the blend.

In general, this research proved that the combinatorial method is effective, efficient, and convenient for evaluating the morphology evolution of polymer blend. All of results present a relatively comprehensive explanation for the formation of the morphology of B-LMWPE/UHMWPE blend films under the temperature gradient. They are useful in understanding the relationship between crystallization and phase separation in the crystalline polymer blend.

Acknowledgment. The authors acknowledge the financial support from the National Natural Science Foundation of China (NSFC) program (No. 20774014).

References and Notes

(1) Smith, P.; Lemstra, P. J.; Kalb, B.; Pennings, A. J. *Polym. Bull.* (*Berlin*) **1979**, *1*, 733–736.
(2) Smith, P.; Lemstra, P. J. *Polymer* **1980**, *21*, 1341–1343.
(3) Smith, P.; Lemstra, P. J.; Booij, H. C. *J. Polym. Sci., Polym. Phys. Ed.* **1981**, *19*, 877–888.
(4) Bin, Y. Z.; Ma, L.; Adachi, R.; Kurosu, H.; Matsuo, M. *Polymer* **2001**, *42*, 8125–8135.
(5) Sawatari, C.; Shimogiri, S.; Matsuo, M. *Macromolecules* **1987**, *20*, 1033–1041.
(6) Sawatari, C.; Matsuo, M. *Polymer* **1989**, *30*, 1603–1614.
(7) Sawatari, C.; Satoh, S.; Matsuo, M. *Polymer* **1990**, *31*, 1456–1463.
(8) Tsai, F. J.; Torkelson, J. M. *Macromolecules* **1990**, *23*, 775–784.
(9) Wachowicz, M.; White, J. L. *Macromolecules* **2007**, *40*, 5433–5440.
(10) Schaaf, P.; Lotz, B.; Wittmann, J. C. *Polymer* **1987**, *28*, 193–200.
(11) Matsuo, M.; Miyoshi, S.; Azuma, M.; Bin, Y. Z.; Agari, Y.; Sato, Y.; Kondo, A. *Macromolecules* **2005**, *38*, 6688–6699.
(12) Graham, P. D.; McHugh, A. J. *Macromolecules* **1998**, *31*, 2565–2568.
(13) Bansil, R.; Lal, J.; Carvalho, B. L. *Polymer* **1992**, *33*, 2961–2969.
(14) Tanaka, H.; Araki, T. *Phys. Rev. Lett.* **1997**, *78*, 4966.
(15) Tanaka, H. *J. Phys.: Condens. Matter* **2000**, *12*, 207–264.
(16) Meredith, J. C.; Karim, A.; Amis, E. J. *Macromolecules* **2000**, *33*, 5760–5762.
(17) Meredith, J. C.; Smith, A. P.; Karim, A.; Amis, E. J. *Macromolecules* **2000**, *33*, 9747–9756.
(18) Smith, A. P.; Douglas, J. F.; Meredith, J. C.; Amis, E. J.; Karim, A. *J. Polym. Sci., Part B: Polym. Phys.* **2001**, *39*, 2141–2158.
(19) Smith, A. P.; Douglas, J. F.; Meredith, J. C.; Amis, E. J.; Karim, A. *Phys. Rev. Lett.* **2001**, *87*, 15503–15503−4.
(20) Crosby, A. J.; Karim, A.; Amis, E. J. *J. Polym. Sci., Part B: Polym. Phys.* **2003**, *41*, 883–891.
(21) Ashley, K. M.; Raghavan, D.; Douglas, J. F.; Karim, A. *Langmuir* **2005**, *21*, 9518–9523.
(22) Matsuo, M.; Sawatari, C. *Macromolecules* **1988**, *21*, 1653–1658.
(23) Matsuo, M.; Sawatari, C. *Macromolecules* **1988**, *21*, 1658–1664.
(24) Matsuo, M.; Ma, L.; Azuma, M.; He, C. Q.; Suzuki, T. *Macromolecules* **2002**, *35*, 3059–3065.
(25) Matsuo, M.; Hashida, T.; Tashiro, K.; Agari, Y. *Macromolecules* **2002**, *35*, 3030–3040.
(26) Matsuo, M.; Kawase, M.; Sugiura, Y.; Takematsu, S.; Hara, C. *Macromolecules* **1993**, *26*, 4461–4471.
(27) Lu, X. Y.; Zhang, J. L.; Zhang, C. C.; Han, Y. C. *Macromol. Rapid Commun.* **2005**, *26*, 637–642.
(28) Sehgal, A.; Karim, A.; Stafford, C.; Fasolka, M. *Microsc. Today* **2003**, *Sept/Oct*, 26–29.
(29) Okinaka, J.; Tran-Cong, Q. *Physica D* **1995**, *84*, 23–30.
(30) Hunt, J. D.; Jackson, K. A.; Brown, H. *Rev. Sci. Instrum.* **1966**, *37*, 805.
(31) Scriven, L. E.; Sternling, C. V. *Nature* **1960**, *187*, 186–188.
(32) Strawhecker, K. E.; Kumar, S. K.; Douglas, J. F.; Karim, A. *Macromolecules* **2001**, *34*, 4669–4672.
(33) Vonk, C. G.; Pijpers, A. P. *J. Polym. Sci., Polym. Phys. Ed.* **1985**, *23*, 2517–2537.
(34) Mandelkern, L. *Rubber Chem. Technol.* **1959**, *32*, 1392.
(35) Moller, K.; Gevert, T. *J. Appl. Polym. Sci.* **1994**, *51*, 895–903.
(36) Graciano-Verdugo, A. Z.; Peralta, E.; Gonzalez-Rios, H.; Soto-Valdez, H. *Anal. Chim. Acta* **2006**, *557*, 367–372.